MATERIALE PLASTICE
https://revmaterialeplastice.ro
https://doi.org/10.37358/Mat.Plast.1964

Optimizing 3D Printing: Enhancing Performance Through Parameter Control

IOANA CATALINA ENACHE, OANA-ROXANA CHIVU, IACOB STEFAN ANDREI*, MARINESCU MARINELA, LARISA BUTU
National University of Science and Technology Politehnica Bucharest, 313 Splaiul Independentei, Bucharest, 060042, Romania

Abstract: *Fused deposition modeling (FDM) is increasingly used to manufacture functional polymer components, but the mechanical performance of printed parts is strongly influenced by process parameters. This study examines the effects of build orientation, infill density, infill pattern, and printing speed on the tensile behavior of polylactic acid (PLA) specimens. Dog-bone samples with ISO 527-2 type 1A geometry were printed using three build orientations (A—horizontal, B—vertical, C—lateral), two infill densities (40% and 70%), two infill patterns (triangle and tri-hexagon), and two printing speeds (40 and 60 mm/s). Tensile tests were performed to determine Young's modulus, yield stress, ultimate tensile strength, and elongation at break. The lateral (C) orientation provided the highest mechanical performance, with an average ultimate tensile strength of 47 MPa and a Young's modulus of 2.9 GPa, compared to 33 MPa ($E \approx 2.4$ GPa) for the horizontal (A) orientation and 16 MPa ($E \approx 2.0$ GPa) for the vertical (B) orientation. For horizontally printed specimens, a 70% infill consistently increased tensile strength relative to 40% infill. The combination of 70% infill, triangular pattern, and 40 mm/s printing speed (A70T40) achieved the highest ultimate tensile strength among the infill configurations. These findings highlight the importance of selecting appropriate printing parameters when PLA components are intended for load-bearing applications.*

Keywords: *Additive manufacturing, PLA, tensile testing, mechanical properties, infill pattern, infill percentage, build orientation*

1. Introduction

3D printing, also known as additive manufacturing, is increasingly used in industrial applications because of its flexibility and efficiency. Unlike traditional production methods, this technology enables the direct fabrication of components from a digital model, eliminating costly steps such as casting, machining, or welding. As a result, significant reductions in time and cost are achieved, along with the ability to quickly adapt product designs [1,2].

One of the major advantages of 3D printing is the high degree of design freedom it offers. Through layer-by-layer deposition, complex structures can be created, including optimized internal geometries such as honeycomb patterns, which combine stiffness with reduced weight. In cases where component dimensions exceed the printer's build volume, they can be produced in segments and subsequently assembled into a single unit [3,4]. The importance of process parameters, internal infill patterns, and surface topography in determining part performance has been highlighted in the specialized literature, including the work *Additive Manufacturing Technologies: 3D Printing, Rapid Prototyping, and Direct Digital Manufacturing* by Gibson et al. [5]. This technology also contributes to shortening the product development cycle, as parts can be manufactured within a few hours or days, depending on complexity and equipment. Precise control of material consumption minimizes waste, making the process more sustainable compared to conventional methods [6].

email: andrei.iacob1@gmail.com

Polylactic acid (PLA) is one of the most commonly used materials in 3D printing by FDM, due to its compatibility with most printers and dimensional stability during cooling. PLA is also notable for its potential biodegradability under appropriate conditions; in particular, it can degrade relatively rapidly in industrial composting environments, whereas in ambient conditions its degradation is much slower [7,8]

Studies have shown that the mechanical performance of PLA components strongly depends on printing parameters such as layer height, infill density and pattern, or deposition speed. The design of internal infill structures is a key factor in improving both the mechanical performance and material efficiency of components produced using FDM technology [7,8]. These variables influence tensile strength and the structural behavior of the parts. Understanding these relationships is essential for process optimization and for adapting components to specific applications [9,10].

In this paper, several parameter sets were analyzed—printing speed, infill density and pattern, as well as build plate orientation—in order to determine the optimal combination that ensures superior mechanical properties and efficient material usage.

3D printing transforms abstract concepts into tangible models and enhances creativity and innovative thinking. However, both from a didactic and an engineering perspective, the use of this technology presents a number of advantages and disadvantages (Table 1).

Table 1. Advantages and disadvantages of 3D printing

Advantages	Disadvantages/Limitations	Article
Transforms abstract concepts into concrete, easily understandable models.	Requires advanced digital and technical skills.	Howell et al., 2020 [11]
Stimulates creativity, imagination, and active learning.	Lack of professional training in the use of 3D technologies.	De la Cruz Campos et al., 2022 [12]
Increase motivation for fields like Science, Technology, Engineering, and Mathematics (STEM) and promotes critical thinking.	Low level of trust in new technologies.	Cheng et al., 2020 [13]
Facilitates collaboration between specialists thru joint projects.	Activities can be time-consuming and delay project planning.	Stevenson et al., 2019 [14]
Can help develop technical skills.	Limited access to digital equipment and infrastructure.	Asempapa & Love, 2021 [15]
Allows the integration of art and design with the exact sciences (STEAM).	Printer and material costs can be high.	Suciu et al., 2019 [16]
Supports project-based learning and design thinking.	Requires specialized technical maintenance and IT support.	Hsu & Ou, 2022 [17]
Helps develop spatial and 3D modeling skills.	Lack of an extensive database for 3D models.	De la Cruz Campos et al., 2022 [12]
Encourages interdisciplinary learning and the application of knowledge from various fields.	Sometimes too much emphasis is placed on the technical aspects, not on the basic scientific concepts.	Forbes et al., 2021 [18]
It allows for the visualization of complex structures (e.g., molecules, organs, geometric models).	Results may vary in high-volume productions due to temperature changes and processing.	Pernaa & Wiedmer, 2020 [19]
It offers increased accessibility—anyone can create 3D models at a low cost.	High accessibility poses legal risks (copyright infringement) and safety risks (the possibility of printing weapons).	Kefalis et al., 2024 [20]

This study provides a relevant basis for future research aimed at understanding the behavior and properties of internal layers in 3D-printed structures. An applicable domains like inverse modeling of natural discontinuities in rocks [21–23], as it concentrated on the impact of 3D printing parameters on the mechanical behavior of PLA specimens. Nowadays, sophisticated 3D printing (3DP) and scanning (3DS) technology combined with computer-aided design (CAD) are creating new avenues for accurately

replicating the surface morphology of natural joints. Still, physical replication accuracy and functionality support strategic control over print parameters, such as print orientation, density, and model.

The present study aims to investigate the influence of several key 3D printing parameters—namely build orientation, infill pattern (triangle vs. tri-hex), infill density (40% vs. 70%), and printing speed (40 vs. 60 mm/s)—on the tensile behavior of PLA (polylactic acid) specimens. Previous studies have shown that smaller layer heights improve interlayer bonding, while higher infill densities and optimized printing speeds enhance stiffness and reduce porosity [24–26]. Understanding how these factors affect mechanical performance is essential for optimizing structural integrity. and efficiency of 3D-printed components.

Based on the expected load-path continuity provided by the filament deposition, we hypothesize that specimens printed in the lateral C-orientation will exhibit higher tensile strength and stiffness than those printed in orientations A (horizontal) and B (vertical). We further hypothesize that higher infill density (70% vs. 40%) and a triangular infill pattern, which creates straighter load paths, will increase ultimate tensile strength compared with tri-hexagonal infill, while printing speed will have a secondary effect within the investigated 40–60 mm/s range.

How these factors affect mechanical performance is essential for optimizing the structural integrity and efficiency of 3D-printed components.

2. Materials and methods

2.1. 3 D printed samples for tensile tests

Autodesk Inventor is a 3D modeling platform designed to support the development and engineering of components across various industrial sectors. Its integrated tools allow not only the creation of precise parametric models but also the virtual testing of component behavior under mechanical loads. In this study, Inventor was used to develop the three-dimensional model of the specimen intended for tensile testing, as well as to perform preliminary mechanical simulations. Figure 1 presents the 3D model of the specimen and its standardized dimensions according to ISO 527 [27], which defines the geometric characteristics and testing conditions for plastic materials.

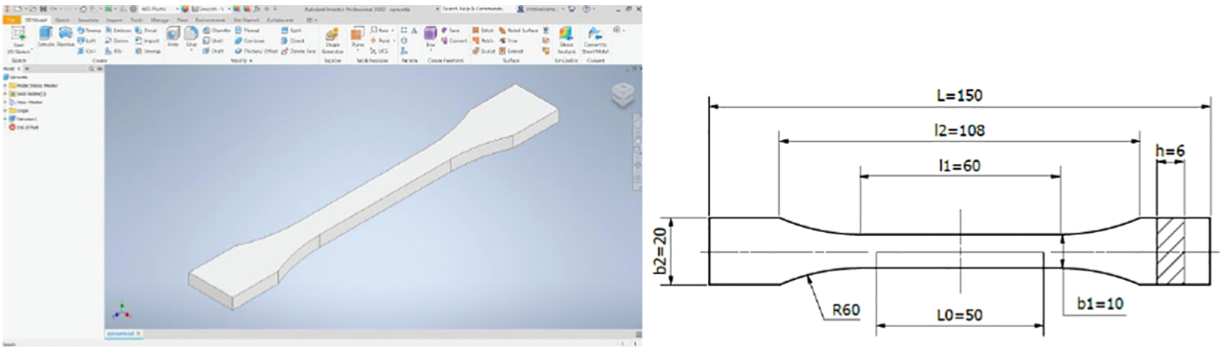

Figure 1. The dumbbell-shaped specimen and the dimensions used

Ultimaker Cura is an advanced, open-source slicing software developed by Ultimaker, designed to prepare 3D models for additive manufacturing. It converts digital 3D models, typically in formats such as STL, OBJ, or 3MF, into G-code instructions that guide 3D printers during the fabrication process [28,29]. This software supports over 500 different 3D printer models through customizable machine profiles.

In this study Ultimaker Cura was used to process the model, imported as an OBJ file, and configure the necessary printing settings. The software's intuitive interface and extensive customization options facilitated the preparation of the model for printing, ensuring optimal print quality and

material efficiency. Figure 2 illustrates the imported 3D model within the Cura interface, displaying the configured settings tailored for the specific printing requirements.

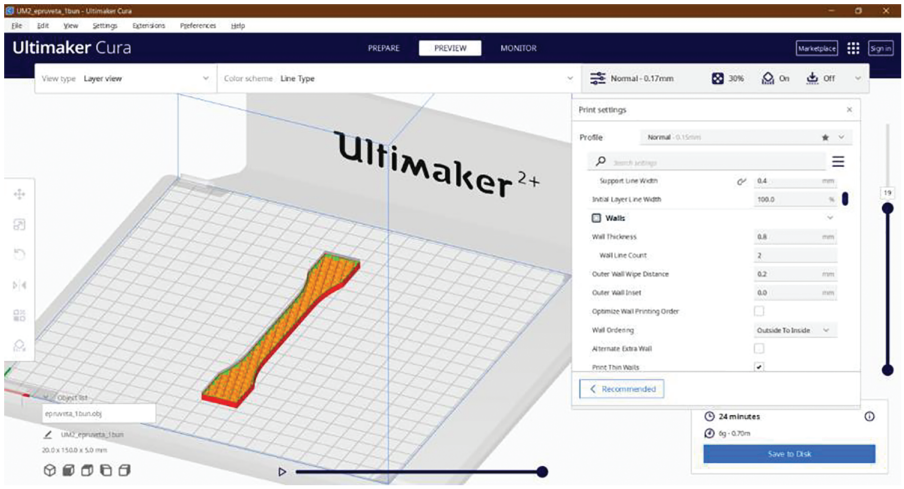

Figure 2. 3D Model of the specimen imported into Ultimaker Cura Software and printing configuration

The design of the tensile test specimen was meticulously crafted to ensure compatibility with the universal testing machine's grip system, facilitating accurate and reproducible mechanical testing. The specimen's geometry and dimensions adhere to established standards, promoting uniform stress distribution and minimizing artifacts during testing.

The specimen's size is optimized to prevent microstructural influences, such as localized crystalline behaviors, from skewing the results. This ensures that the measured elongation accurately reflects the material's intrinsic properties.

A homogeneous stress field is maintained within the gauge section, achieved by designing the specimen with appropriate shoulder lengths and fillet radii. This configuration reduces stress concentrations at the grips, ensuring that deformation occurs uniformly in the central region.

Maintaining a uniform stress state is crucial for accurately identifying the onset of plastic deformation on the stress-strain curve. This uniformity simplifies the calculation of engineering stresses and strains, providing reliable data for material characterization.

The objective of this study is to analyze how build orientation, infill pattern (triangle vs. tri-hex) (Figure 3), infill density (40% vs. 70%), and printing speed (40 vs. 60 mm/s) influence the tensile behavior of PLA specimens.

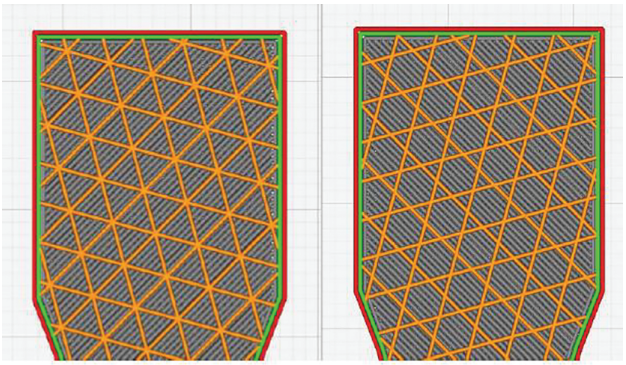

Figure 3. The printing pattern for a 40% infill density using the Tri-Hexagon and Triangle fill patterns

Figure 4 illustrates the three primary printing orientations considered:

- A (Horizontal): The specimen is printed parallel to the build plate, with layers oriented in the X-Y plane.
- B (Vertical): The specimen is printed perpendicular to the build plate, with layers oriented along the Z-axis.
- C (Lateral): The specimen is printed at an intermediate angle, typically 45°, relative to the build plate.

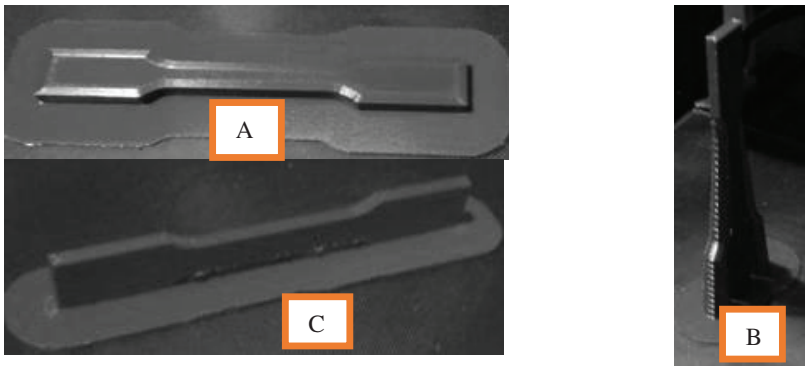

Figure 4. Directions of printing tensile samples

Each orientation affects the bonding between layers and the resultant mechanical properties. For instance, printing along the Z-axis (orientation B) often results in weaker interlayer adhesion due to the nature of the deposition process, potentially leading to reduced tensile strength. Conversely, orientations A and C can enhance interlayer bonding, improving overall mechanical performance.

Understanding the implications of printing orientation (Figure 4) is essential for optimizing the mechanical properties of 3D printed specimens. By selecting the appropriate orientation, one can tailor the specimen's characteristics to meet specific testing requirements.

For each printing orientation, five specimens were manufactured using 3D printing. Additionally, to analyze other parameters such as infill density, infill pattern, and printing speed, 16 additional specimens were produced, as presented in Table 1. Three specimens from each category were fabricated using 3D printing, with all specimens being consistently oriented in direction A to ensure uniformity in the experimental setup.

FDM sample properties depend strongly on printing parameters. For all samples, the printing parameters were carefully controlled and kept constant unless otherwise stated: layer height 0.20 mm, extrusion width 0.40 mm, and nozzle diameter 0.40 mm, the infill line distance was 0.40 mm. The printing temperature was 200°C, the bed temperature 60°C, and the ambient laboratory temperature (23 ± 2)°C. Each specimen was printed individually to avoid cooling-related inconsistencies and to ensure a uniform thermal history. The specimen coding used for infill parameters is shown in Table 2.

Table 2. Test sample coding

Code	Degree of filling	Filling paterns	Print speed
A70T60	70%	Triangle	60 mm/s
A70H60	70%	Tri-hexagon	60 mm/s
A70T40	70%	Triangle	40 mm/s
A70H40	70%	Tri-hexagon	40 mm/s
A40T60	40%	Triangle	60 mm/s
A40H60	40%	Tri-hexagon	60 mm/s
A40T40	40%	Triangle	40 mm/s
A40H40	40%	Tri-hexagon	40 mm/s

2.2. Tensile tests

Tensile testing was conducted using an INSTRON 5982 universal testing machine, with data acquisition and analysis performed through BlueHill software. The mechanical properties evaluated during the tests included elongation at break, Young's modulus, ultimate tensile strength, and the maximum force applied at the point of fracture.

Tensile strength (σ_r), often called rupture strength, is defined as the stress corresponding to the highest recorded force after the material has passed its yield point. Fracture occurs when the material can no longer sustain the applied load, typically at a stress slightly lower than the peak tensile strength.

For each group of specimens, statistical analyses were performed to quantify variability, including calculations of the mean absolute deviation and standard deviation, providing insight into the consistency of the results.

The stress experienced by the specimen was calculated using the standard formula:

$$\sigma = \frac{F}{A} \text{ (Mpa)}$$

where F represents the force measured by the load cell, and A is the cross-sectional area of the specimen.

Tensile testing was conducted using an INSTRON 5982 universal testing machine, with data acquisition and analysis performed through BlueHill software. The mechanical properties evaluated were Young's modulus (E), apparent yield stress (σ_c), ultimate tensile strength (σ_r), and elongation at break (ε_B). All tests were carried out at (23 ± 2)°C and (50 ± 10)% relative humidity.

The tensile specimens followed the ISO 527-2 standard for plastics (type 1A geometry), with a nominal gauge length L0 = 50 mm, gauge width 10 mm, and thickness 4 mm. Prior to testing, the actual gauge width and thickness of each specimen were measured in the gauge section using a digital caliper, and the corresponding cross-sectional area A was used in the stress calculations.

Engineering stress σ was calculated from the measured force F using σ = F/A. Engineering strain ε was obtained from the axial extension measured by the testing machine's clip-on extensometer attached to the gauge section and computed as $\varepsilon = \Delta L/L0$. The crosshead speed was set to 5 mm/min, in accordance with ISO 527 recommendations for quasi-static tensile testing of thermoplastics.

Tensile strength (σ_r), often called rupture strength, is defined here as the maximum engineering stress recorded on the stress–strain curve. The apparent yield stress σ_c reported in the tables corresponds to the 0.2% offset stress σM0.2 defined in ISO 527. It was obtained by constructing a line parallel to the initial linear elastic portion of the stress–strain curve, offset by 0.2% strain, and determining its intersection with the experimental curve. This methodology ensures a comprehensive assessment of the material's mechanical performance under tensile loading and enables comparisons across different printing orientations, infill densities, and internal structures.

3. Experimental results

The results of tensile tests for the samples made of PLA, for the three printing directions are presented in the tables below (Tables 3–5).

Table 3. Results test for PLA, printing position A

Code	E	γ	σ_c	σ_r
	(MPa)	(-)	(MPa)	(MPa)
A01-PLA	2320	0.336	32.789	37.041
A02-PLA	2518	0.351	30.479	33.716
A03-PLA	2510	0.329	26.653	26.653
A04-PLA	2525	0.327	31.379	33.882
A05-PLA	2266	0.325	29.998	33.630
Average	2428	0.334	30.260	32.986
StDev	124.404	0.010	2.279	3.188
Coefficient of variation%	5.124	3.038	7.532	11.576

Table 4. Results test for PLA, printing position B

Code	E	γ	σ_c	σ_r
	(MPa)	(-)	(MPa)	(MPa)
B01-PLA	1957	0.223	17.250	17.250
B02-PLA	1956	0.225	17.251	17.251
B03-PLA	1951	0.215	14.296	14.296
B04-PLA	1981	0.234	14.642	14.642
B05-PLA	2213	0.236	18.635	18.635
Average	2012	0.227	16.41	16.41
StDev	113.185	0.0086	1.868	1.868
Coefficient of variation%	5.627	3.778	11.380	11.380

Table 5. Results test for PLA, printing position C

Code	E	γ	σ_c	σ_r
	(MPa)	(-)	(MPa)	(MPa)
C01-PLA	2954	0.348	45.307	48.297
C02-PLA	2886	0.341	44.846	46.839
C03-PLA	2970	0.543	45.806	47.451
C04-PLA	2817	0.191	46.806	47.309
C05-PLA	2940	0.323	44.094	47.148
Average	2913	0.349	45.372	47.416
StDev	62.638	0.126	1.020	0.542
Coefficient of variation%	2.150	36.043	2.248	1.144

The mechanical test results for PLA samples show significant variations depending on the printing orientation. In position A (horizontal) (Table 3), the average values obtained were: elastic modulus

E = 2428 MPa, elongation at break $\gamma = 0.334$, yield strength $\sigma_c = 30.26$ MPa, and tensile strength $\sigma_r = 32.99$ MPa. These results indicate balanced mechanical behavior, with moderate tensile strength and good ductility.

For position B (vertical) (Table 4), the average values are considerably lower: E = 2012 MPa, $\gamma = 0.227$, $\sigma_c = 16.41$ MPa, and $\sigma_r = 16.41$ MPa (n = 5). This demonstrates that the vertical orientation significantly reduces mechanical strength, as the layer-by-layer deposition is more prone to weaknesses under tensile loading.

In contrast, the samples printed in position C (lateral) (Table 5) exhibited the best performance: E = 2913 MPa, $\gamma = 0.349$, $\sigma_c = 45.37$ MPa, and $\sigma_r = 47.42$ MPa. These values highlight a significant increase in stiffness and tensile strength, confirming that this orientation promotes better interlayer cohesion and a more uniform stress distribution.

Therefore, among the three orientations, position C provides the highest mechanical performance, followed by position A, while position B shows the lowest values. This behavior confirms the decisive influence of printing orientation on the mechanical performance of FDM-manufactured PLA components.

Correspondingly, Figure 5 provides the average engineering stress–strain curves for the PLA tensile specimens in build orientations A, B, and C.

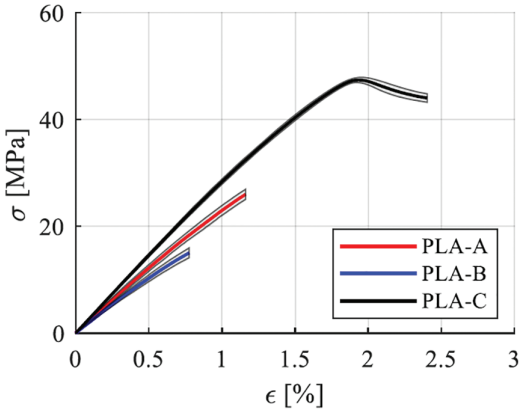

Figure 5. Representative engineering stress–strain curves for tensile specimens printed in orientations A (horizontal), B (vertical), and C (lateral)

The tensile strength values for the specimens printed in position A, for which the process parameters—printing speed, infill density, and printing pattern—were varied, are presented in Table 5. These values provide a detailed insight into the influence of each parameter on the mechanical behavior of the material used. A comparative analysis of these data enables the identification of optimal printing configurations that ensure superior mechanical strength, thus contributing to the improvement of the additive manufacturing process and the optimization of the properties of the fabricated parts.

In Figure 6, the variation of the average ultimate tensile strength is observed. It represents the stress corresponding to the maximum force recorded during the test after exceeding the yield limit. The highest tensile strength is observed in the 70T40 specimen set, with a value of 28.46 MPa, corresponding to the maximum applied force of 1.47 kN. The lowest value is recorded for the 40T60 specimen set, with a corresponding applied force of 1.15 kN. Therefore, the tensile strength is directly proportional to the applied force.

Figure 6 presents the ultimate tensile strength for the eight parameter combinations coded in Table 6 (A40H40–A70T60). The bars show mean values and the error bars represent one standard deviation (mean ± SD, n = 3 specimens per condition). The highest tensile strength is observed for the A70T40

specimen set, with a value of 28.46 MPa, corresponding to a maximum applied force of 1.47 kN, whereas the lowest value is recorded for the A40T60 specimen set (22.51 MPa, 1.15 kN). These results highlight the combined influence of infill density, infill pattern, and printing speed on the mechanical response of PLA.

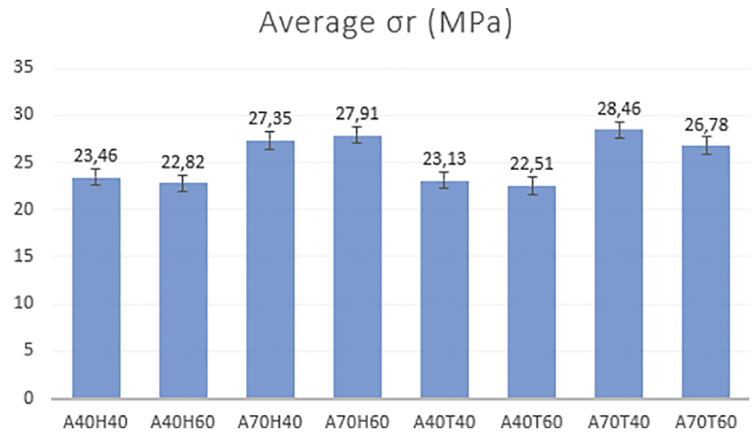

Figure 6. Ultimate tensile strength of PLA specimens for the different infill densities, infill patterns, and printing speeds (mean ± SD, n = 3 for each condition)

Table 6. Results test for PLA, different infill process parameters

Code	Average σ_r	StDev
	(MPa)	(MPa)
A40H40	23.46	1.11
A40H60	22.82	0.45
A70H40	27.35	0.61
A70H60	27.91	1
A40T40	23.13	0.79
A40T60	22.51	0.08
A70T40	28.46	0.25
A70T60	26.78	0.01

4. Discussion

The results confirm the strong anisotropy of FDM-printed PLA and demonstrate that build orientation is the dominant parameter influencing tensile performance. Among the three orientations investigated, the lateral C-orientation yielded the highest ultimate tensile strength ($\sigma_r \approx 47$ MPa) and stiffness (E ≈ 2.9 GPa), followed by the horizontal A-orientation ($\sigma_r \approx 33$ MPa, E ≈ 2.4 GPa) and the vertical B-orientation ($\sigma_r \approx 16$ MPa, E ≈ 2.0 GPa). This trend can be explained by the relative orientation of deposited filaments and interlayer interfaces with respect to the loading direction. In the lateral and horizontal configurations, a larger fraction of filaments is aligned with the tensile axis, promoting more effective load transfer and reducing the likelihood of interlayer debonding. In contrast, for the vertical orientation the load is largely perpendicular to the layer interfaces, so failure is dominated by interlayer separation rather than intrinsic filament strength.

The infill study on horizontally printed specimens further highlights the importance of internal architecture. Increasing infill density from 40% to 70% systematically enhanced ultimate tensile strength for both triangular and tri-hexagon patterns, as reflected in Table 6 and Figure 6. This behavior is consistent with the reduction of internal porosity and the increase in effective load-bearing cross-section at higher infill levels. At 70% infill, the A70T40 configuration (triangular infill at 40 mm/s) reached the highest ultimate tensile strength (28.46 MPa), while the A70T60 and A70H60 conditions yielded slightly lower values. At 40% infill, all configurations showed reduced strength, with the minimum σ_r observed for A40T60 (22.51 MPa).

For specimens with a 70% infill density, the maximum tensile strength is obtained for the A70T40 condition (triangle infill, 70% density, 40 mm/s), with $\sigma_r = 28.46$ MPa, whereas the lowest value corresponds to the A70T60 condition (triangle infill, 70% density, 60 mm/s). For specimens with a 40% infill density, the highest tensile strength is achieved for the A40H40 condition (tri-hexagonal infill, 40% density, 40 mm/s, $\sigma_r = 23.46$ MPa), while the lowest value is recorded for A40T60 (triangle infill, 40% density, 60 mm/s, $\sigma_r = 22.51$ MPa). These results indicate that, within the investigated range, the lower printing speed (40 mm/s) tends to promote higher tensile strength for both infill levels

The comparison between infill patterns indicates that the triangular structure tends to provide slightly higher or comparable tensile strength to the tri-hexagon pattern at 70% infill, whereas at 40% infill the differences are small. This behavior can be attributed to the straighter load paths and higher stiffness provided by the triangular infill, which efficiently carries tensile and compressive stresses along the filament trajectories. By contrast, the tri-hexagon pattern introduces more inclined and curved paths, which can increase deformation capacity and energy absorption. This is consistent with the higher elongation at break generally observed for the tri-hexagon structures, making them attractive for applications where toughness and flexibility are more important than maximum strength.

Within the investigated range, printing speed had a secondary but noticeable effect on mechanical behavior. The lower speed (40 mm/s) generally favored higher tensile strength, particularly at 70% infill, which suggests that the longer residence time and more stable thermal conditions can improve interlayer bonding and dimensional accuracy. At higher speed (60 mm/s), the reduced time for filament fusion may slightly diminish the quality of interlayer adhesion, especially in highly filled geometries. However, the magnitude of this effect remains modest compared with the influence of orientation and infill density.

A limitation of the present study is the moderate sample size per parameter set ($n = 3$ per condition), which restricts the statistical power of the analysis. Nevertheless, the observed trends are consistent across orientations and infill configurations and align with previous studies on FDM-printed PLA. Future work should increase the number of specimens, extend the parameter space (e.g., layer height, nozzle temperature), and include other loading modes such as fatigue, impact, and time-dependent behavior. In addition, investigating different materials and post-processing treatments would further clarify how process parameters can be tailored to achieve the desired balance between strength, stiffness, and ductility in 3D-printed components.

5. Conclusions

This study quantified the effect of build orientation, infill density, infill pattern, and printing speed on the tensile behavior of FDM-printed PLA specimens. The results demonstrate that printing orientation is the dominant factor controlling mechanical performance. Among the three orientations investigated, the lateral C-orientation yielded the highest tensile properties ($\sigma_r \approx 47$ MPa, $E \approx 2.9$ GPa), followed by the horizontal A-orientation ($\sigma_r \approx 33$ MPa), whereas the vertical B-orientation exhibited the lowest strength ($\sigma_r \approx 16$ MPa). These findings confirm that aligning the filament paths and interlayer bonds with the load direction is essential for maximizing tensile strength and stiffness.

For horizontally printed specimens, increasing infill density from 40% to 70% systematically improved ultimate tensile strength for both infill patterns. The best-performing configuration was

A70T40 (70% infill, triangular pattern, 40 mm/s), which achieved $\sigma_r = 28.46$ MPa and an applied force of 1.47 kN, while the weakest configuration was A40T60 ($\sigma_r = 22.51$ MPa, 1.15 kN). The triangular infill generally provided slightly higher or comparable tensile strength to the tri-hexagon pattern at 70% infill, whereas the tri-hexagon structure tended to exhibit higher elongation at break, indicating enhanced energy absorption capability.

Within the tested range, printing speed had a secondary influence compared with orientation and infill density, with the lower speed (40 mm/s) typically associated with higher tensile strength. Overall, the combined effect of orientation, infill density, infill pattern, and printing speed must be considered when designing PLA components for load-bearing applications.

From a practical standpoint, for tensile-loaded PLA parts we recommend using the lateral (C) orientation to maximize interlayer strength, together with relatively high infill density and a stiff infill pattern (such as triangle) where strength is the primary requirement. Future research should investigate a wider range of process parameters, different materials, and additional mechanical tests to further refine design guidelines for functional FDM components.

Acknowledgement: Not applicable.

Funding Statement: This work was supported by the National Program for Research of the National Association of Technical Universities (GNAC-ARUT 2023).

Author Contributions: The authors confirm contribution to the paper as follows: study conception and design: Ioana-Catalina Enache, Oana-Roxana Chivu; data collection: Iacob Stefan Andrei, Marinescu Marinela, Larisa Butu; analysis and interpretation of results: Ioana-Catalina Enache, Marinescu Marinela; draft manuscript preparation: Ioana-Catalina Enache, Oana-Roxana Chivu. All authors reviewed the results and approved the final version of the manuscript.

Availability of Data and Materials: The data that support the findings of this study are available from the corresponding author, [Iacob Stefan Andrei], upon reasonable request.

Ethics Approval: Not applicable.

Conflicts of Interest: We confirm that there are no known conflicts of interest associated with this publication and there has been no significant financial support for this work that could have influenced its outcome.

References

1. Tabassum T, Mir AA. A review of 3D printing technology-the future of sustainable construction. Mater Today Proc. 2023;93:408–14. doi:10.1016/j.matpr.2023.08.013.
2. Minguella-Canela J, Planas SM, Gomà Ayats JR, de los Santos López MA. Study and comparison of the different costs' schema associated to geometry, material and processing between 3D printing, injection molding and machining manufacturing technologies. Procedia Manuf. 2019;41:280–7. doi:10.1016/j.promfg.2019.09.010.
3. Zhai C, Wang J, Paul Tu Y, Chang G, Ren X, Ding C. Robust optimization of 3D printing process parameters considering process stability and production efficiency. Addit Manuf. 2023;71:103588. doi:10.1016/j.addma.2023.103588.
4. Yan Z, Rahimizadeh A, Zhang Y, Zhou Y, Lessard L. A finite element model for 3D printed recycled parts from end-of-life wind turbine blades. Compos Struct. 2023;320:117177. doi:10.1016/j.compstruct.2023.117177.
5. Gibson I, Rosen D, Stucker B. Additive manufacturing technologies: 3D printing, rapid prototyping, and direct digital manufacturing. 2nd ed. New York, NY, USA: Springer; 2015. doi:10.1007/978-1-4939-2113-3.

6. Shahzad Q, Wang X, Wang W, Wan Y, Li G, Ren C, et al. Coordinated adjustment and optimization of setting time, flowability, and mechanical strength for construction 3D printing material derived from solid waste. Constr Build Mater. 2020;259:119854. doi:10.1016/j.conbuildmat.2020.119854.
7. Mourya V, Bhore SP, Wandale PG. Multiobjective optimization of tribological characteristics of 3D printed texture surfaces for ABS and PLA Polymers. J Thermoplast Compos Mater. 2024;37(2):772–99. doi:10.1177/08927057231185710.
8. Hamed MA, Abbas TF. The impact of FDM process parameters on the compression strength of 3D printed PLA filaments for dental applications. Adv Sci Technol Res J. 2023;17(4):121–9. doi:10.12913/22998624/169468.
9. Mishra A, Kumar M, Kumar R, Kumar Sharma A. An investigation on tensile strength of 3D printed parts of Acrylonitrile butadiene styrene (ABS) material. Mater Today Proc. 2024;113:247–51. doi:10.1016/j.matpr.2023.09.088.
10. Khan I, Tariq M, Abas M, Shakeel M, Hira F, Al Rashid A, et al. Parametric investigation and optimisation of mechanical properties of thick tri-material based composite of PLA-PETG-ABS 3D-printed using fused filament fabrication. Compos Part C Open Access. 2023;12:100392. doi:10.1016/j.jcomc.2023.100392.
11. Howell ME, Booth CS, Sikich SM, Helikar T, van Dijk K, Roston RL, et al. Interactive learning modules with 3D printed models improve student understanding of protein structure-function relationships. Biochem Mol Biol Educ. 2020;48(4):356–68. doi:10.1002/bmb.21362.
12. De la Cruz Campos JC De, Soto MN, Jiménez CR, Navas-Parejo MR. Impresión 3D en educación. Perspectiva teórica y experiencias en el aula. Rev CENTRA De Cienc Soc. 2022;2022:67–80. doi:10.54790/rccs.16.
13. Cheng L, Antonenko PD, Ritzhaupt AD, Dawson K, Miller D, MacFadden BJ, et al. Exploring the influence of teachers' beliefs and 3D printing integrated STEM instruction on students' STEM motivation. Comput Educ. 2020;158:103983. doi:10.1016/j.compedu.2020.103983.
14. Stevenson M, Bower M, Falloon G, Forbes A, Hatzigianni M. By design: professional learning ecologies to develop primary school teachers' makerspaces pedagogical capabilities. Brit J Educational Tech. 2019;50(3):1260–74. doi:10.1111/bjet.12743.
15. Asempapa RS, Love TS. Teaching math modeling through 3D-printing: examining the influence of an integrative professional development. Sch Sci Math. 2021;121(2):85–95. doi:10.1111/ssm.12448.
16. Suciu A, Buruiană A, Repanovici A, Cotoros D, Bou SF. Pedagogical methods for teaching the use of prototyping by 3D printers. Procedia Manuf. 2019;32(1):356–9. doi:10.1016/j.promfg.2019.02.225.
17. Hsu CY, Ou SJ. Innovative practice of sustainable landscape architecture education—parametric-aided design and application. Sustainability. 2022;14(8):4627. doi:10.3390/su14084627.
18. Forbes A, Falloon G, Stevenson M, Hatzigianni M, Bower M. An analysis of the nature of young students' STEM learning in 3D technology-enhanced makerspaces. Early Educ Dev. 2021;32(1):172–87. doi:10.1080/10409289.2020.1781325.
19. Pernaa J, Wiedmer S. A systematic review of 3D printing in chemistry education-analysis of earlier research and educational use through technological pedagogical content knowledge framework. Chem Teach Int. 2020;2(2):20190005. doi:10.1515/cti-2019-0005.
20. Kefalis C, Skordoulis C, Drigas A. The role of 3D printing in science, technology, engineering, and mathematics (S.T.E.M.) education in general and special schools. Int J Onl Eng. 2024;20(12):4–18. doi:10.3991/ijoe.v20i12.48931.
21. Jiang Q, Feng X, Gong Y, Song L, Ran S, Cui J. Reverse modelling of natural rock joints using 3D scanning and 3D printing. Comput Geotech. 2016;73(1):210–20. doi:10.1016/j.compgeo.2015.11.020.

22. Niu Q, Jiang L, Li C, Zhao Y, Wang Q, Yuan A. Application and prospects of 3D printing in physical experiments of rock mass mechanics and engineering: materials, methodologies and models. Int J Coal Sci Technol. 2023;10(1):5. doi:10.1007/s40789-023-00567-8.
23. Huang M, Hong C, Sha P, Du S, Luo Z, Tao Z. Method for visualizing the shear process of rock joints using 3D laser scanning and 3D printing techniques. J Rock Mech Geotech Eng. 2023;15(1):204–15. doi:10.1016/j.jrmge.2022.02.013.
24. Gonzalez YE, Mendoza JM, Durán JR, Vertel LCT, Rhenals-Julio JD. Effect of printing parameters on mechanical properties and processing time of additively manufactured parts. Matéria. 2023;28(3):e20230111. doi:10.1590/1517-7076-rmat-2023-0111.
25. Blais P, Toubal L, Zitoune R. The influence of the hole-generation process on fatigue response of open-hole and assembled titanium samples. J Manuf Process. 2024;110:412–23. doi:10.1016/j.jmapro.2024.01.007.
26. Shuai MK, Gong Y, Cheng F, Zhang J, Li RB, Pan J, et al. Innovation in lifetime prediction of rigid polyurethane foam through random vibration and comparison with conventional methods. Polym Test. 2023;125:108122. doi:10.1016/j.polymertesting.2023.108122.
27. ISO 527. Tensile test on plastics. Geneva, Switzerland: International Standard (ISO); 2019.
28. Prodan D, Bucuresteanu A, Motomancea A. Construction of plastic parts on CNC engraving machines and 3D printers. MatPlast. 2018;55(1):75–8. doi:10.37358/mp.18.1.4966.
29. Bryła J, Martowicz A. Study on the importance of a slicer selection for the 3D printing process parameters via the investigation of G-code readings. Machines. 2021;9(8):163. doi:10.3390/machines9080163.

Received: 31 August 2025; Accepted: 12 December 2025; Published: 31 December 2025